

LETTERS

Optimized dynamical decoupling in a model quantum memory

Michael J. Biercuk^{1,2*}, Hermann Uys^{1,3*}, Aaron P. VanDevender¹, Nobuyasu Shiga^{1†}, Wayne M. Itano¹ & John J. Bollinger¹

Any quantum system, such as those used in quantum information or magnetic resonance, is subject to random phase errors that can dramatically affect the fidelity of a desired quantum operation or measurement¹. In the context of quantum information, quantum error correction techniques have been developed to correct these errors, but resource requirements are extraordinary. The realization of a physically tractable quantum information system will therefore be facilitated if qubit (quantum bit) error rates are far below the so-called fault-tolerance error threshold¹, predicted to be of the order of 10^{-3} – 10^{-6} . The need to realize such low error rates motivates a search for alternative strategies to suppress dephasing in quantum systems². Here we experimentally demonstrate massive suppression of qubit error rates by the application of optimized dynamical decoupling^{3–8} pulse sequences, using a model quantum system capable of simulating a variety of qubit technologies. We demonstrate an analytically derived pulse sequence⁹, UDD, and find novel sequences through active, real-time experimental feedback. The latter sequences are tailored to maximize error suppression without the need for a priori knowledge of the ambient noise environment, and are capable of suppressing errors by orders of magnitude compared to other existing sequences (including the benchmark multi-pulse spin echo^{10,11}). Our work includes the extension of a treatment to predict qubit decoherence^{12,13} under realistic conditions, yielding strong agreement between experimental data and theory for arbitrary pulse sequences incorporating nonidealized control pulses. These results demonstrate the robustness of qubit memory error suppression through dynamical decoupling techniques across a variety of qubit technologies^{11,14–16}.

We consider classical phase randomization of a qubit due to the action of the environment as the dominant source of memory errors. Accordingly, we may write a Hamiltonian as $H = \frac{\hbar}{2}[\Omega + \beta(t)]\hat{\sigma}_Z$, where Ω is the unperturbed qubit splitting, β is a classical random variable^{13,17}, and $\hat{\sigma}_Z$ is a Pauli operator. As in ref. 13, we may write the time evolution of a superposition state initially oriented along \hat{Y} under the influence of this Hamiltonian as

$$|\Psi(t)\rangle = \frac{1}{\sqrt{2}} \left(e^{-i\Omega t/2} e^{-\frac{i}{2} \int_0^t \beta(t') dt'} |\uparrow\rangle + e^{i\Omega t/2} e^{\frac{i}{2} \int_0^t \beta(t') dt'} |\downarrow\rangle \right)$$

with $|\uparrow\rangle$ and $|\downarrow\rangle$ the qubit basis states. The term $\beta(t)$ adds a random phase between the basis states in the rotating frame. Accumulation of such a random phase results in decoherence, as an observer loses track of the position of the Bloch vector in the equatorial plane. However, the application of a π pulse around \hat{X} (henceforth denoted π_X), at time $t' = t/2$, will result in the approximate time-reversal of phase accumulation, so long as fluctuations in β are slow relative to the allowed free-precession time of the qubit. This is the basis of the

Hahn spin echo, a fundamental technique for preserving coherence in nuclear magnetic resonance and electron spin resonance systems¹⁰.

Given an arbitrary noise power spectrum $S_\beta(\omega)$, we would expect the Hahn echo to act as a high-pass filter, mitigating phase errors associated with slowly varying Fourier components of β . It was

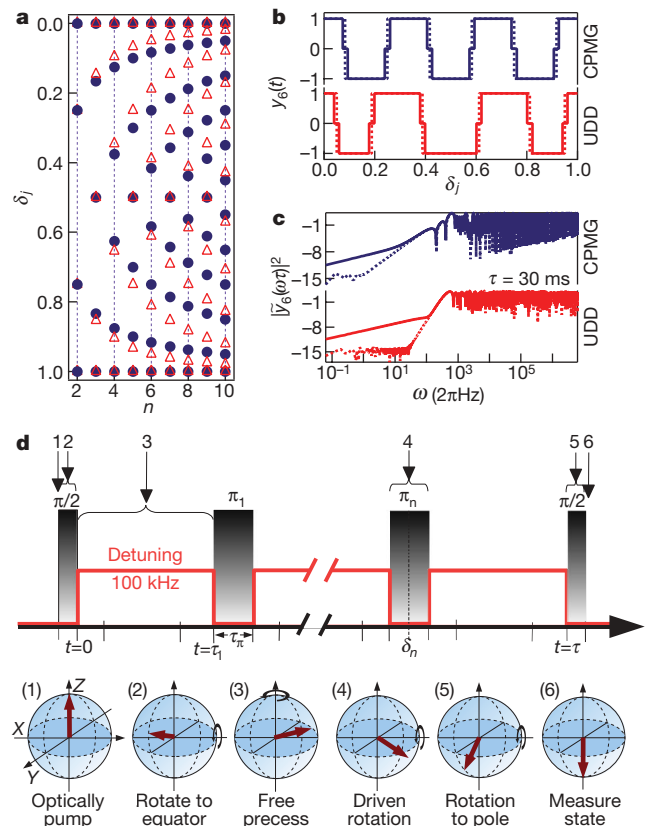


Figure 1 | CPMG and UDD pulse sequence schematics. **a**, Fractional pulse locations, δ_j , of CPMG (filled symbols) and UDD (open symbols) sequences as a function of pulse number, n : $\delta_j^{\text{UDD}} = \sin^2(\pi j / (2n + 2))$. **b**, Examples of the time-domain filter function, $y_6(t)$, for the CPMG and UDD pulse sequences with 6 π -pulses. The dotted line represents the time-domain filter function assuming delta-function π pulses, while the solid line represents the time-domain filter function accounting for non-zero τ_π . **c**, Logarithmic plot of the filter function, $F(\omega\tau) = |y_6(\omega\tau)|^2$, for sequence length $\tau = 30$ ms, and $\tau_\pi = 185$ μ s. Dotted lines indicate filter function with delta-function π pulses, solid lines account for nonzero τ_π . **d**, Generalized diagram of an experimental sequence showing key procedures and designations of key times.

¹NIST Time and Frequency Division, Boulder, Colorado, 80305, USA. ²Georgia Institute of Technology, Atlanta, Georgia, 30332, USA. ³Council for Scientific and Industrial Research, Pretoria, 0001, South Africa. [†]Present address: NICT, Tokyo, Japan.

*These authors contributed equally to this work.

shown previously that this general interpretation can be extended to multipulse sequences: following refs 12 and 13, for any n -pulse sequence of total qubit evolution time τ , the coherence of the state is given as $W(\tau) = \overline{|\langle \sigma_Y \rangle(\tau)|} = e^{-\chi(\tau)}$, where angle brackets indicate an expectation value, and the overbar indicates an ensemble average. In this expression,

$$\chi(\tau) = \frac{2}{\pi} \int_0^{\infty} \frac{S_{\beta}(\omega)}{\omega^2} F(\omega\tau) d\omega$$

where the filter function $F(\omega\tau)$ contains all information about how the pulse sequence will preserve qubit coherence under the influence of $S_{\beta}(\omega)$. $F(\omega\tau)$ is calculated from $F(\omega\tau) = |\tilde{y}_n(\omega\tau)|^2$, where $\tilde{y}_n(\omega\tau)$ is the Fourier transform of the time-domain filter function, $y_n(t)$ (Fig. 1b and c). The time domain filter function alternates between $+1$ and -1 for successive free precession periods.

We begin by studying two distinct pulse sequences, as will be described in order below: CPMG and UDD (pulse spacings illustrated in Fig. 1a). CPMG, after Carr, Purcell, Meiboom and Gill, is an extension of the Hahn spin echo to a multipulse form, incorporating evenly spaced π pulses about an axis rotated 90° from the direction imparting the initial $(\pi/2)_x$ (Fig. 1d). This sequence has been shown to be robust against a variety of phase and rotation errors, and does a particularly good job at refocusing the Bloch vector³.

The UDD, or Uhrig dynamical decoupling, sequence is based on Uhrig's discovery⁹ that for an n -pulse sequence, it is possible to modify the form of the filter function, and hence the efficiency of noise suppression compared to CPMG, simply by changing the relative positions of the pulses within the sequence (Fig. 1a and c). By enforcing certain constraints on the filter function, he developed a novel sequence in the context of the spin boson model (appropriate for

many solid-state systems), designed to increase the suppression of errors at short times—the so-called 'high-fidelity' regime (the UDD sequence was later shown to be general^{13,16,18}).

It is important to understand the performance of a given decoupling sequence in various noise environments, as the experimental noise spectrum can vary significantly between qubit implementations (as in semiconducting quantum dots versus ultracold atoms). For example, in superconducting qubit systems^{13,19,20}, fluctuating electric charges and spin centres produce noise spectra varying as $1/\omega$. By contrast, a spin-boson model predicts noise with an Ohmic spectrum, $S_{\beta}(\omega) \propto \omega$, and a sharp cut-off^{2,21}. In order to test the efficacy of any pulse sequence, one must develop a method and testbed capable of exhibiting a variety of realistic noise environments. In this manner we may think of the testbed as being a model quantum memory capable of simulating other technologies.

We realize such a model quantum memory in an array of $\sim 1,000$ $^9\text{Be}^+$ ions in a Penning ion trap²². Previous experiments have demonstrated that under appropriate conditions these ions form two- or three-dimensional arrays with well defined crystal structure^{23–25} (Fig. 2a inset). The qubit states are realized using a ground-state electron-spin-flip transition (Fig. 2a, also Supplementary Information). Coherent qubit operations are achieved by directly driving this ~ 124 GHz transition via a quasi-optical microwave system (Fig. 2b), which we report here for the first time (Figs 1d, 2c–e). Microwave qubit control is particularly well-suited to dynamical decoupling studies compared to laser-mediated qubit rotations owing to the absence of spontaneous emission in the microwave/millimetre-wave regime. However, the qubit states are highly susceptible to magnetic field fluctuations (states diverge as $\pm\mu_B$, with μ_B the Bohr magneton), making magnetic field noise a significant source of qubit decoherence, and limiting coherence times relative to so-called 'clock' transitions used in precision metrology.

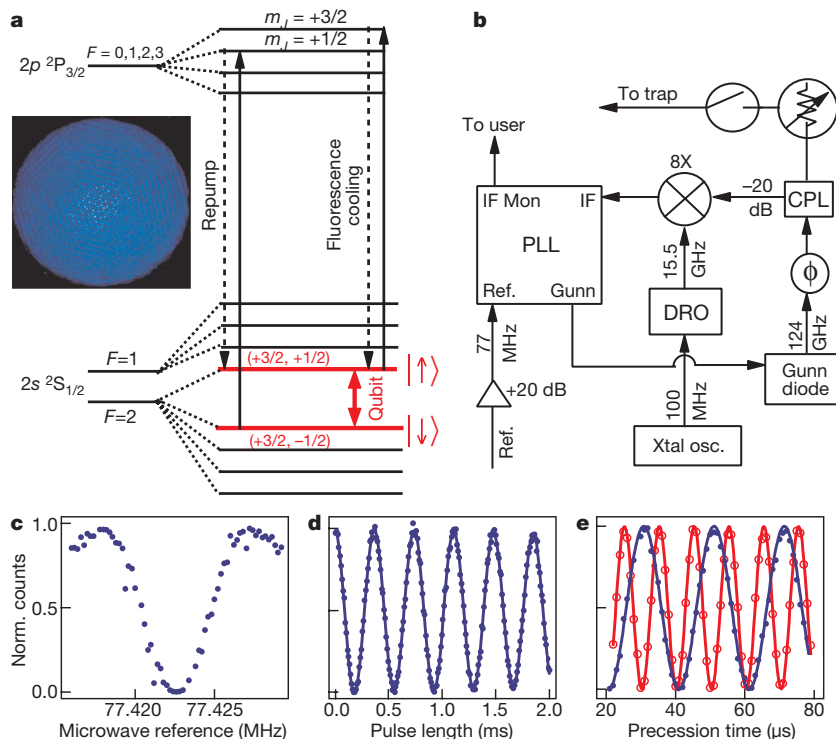


Figure 2 $^9\text{Be}^+$ qubit structure and coherent control. Details are given in Supplementary Information. **a**, Relevant atomic structure at 4.5 T. Qubit states are labelled with (m_I, m_J) , respectively the nuclear and electron spin projections of the atom along the quantization axis. Inset, strobbed optical image of ion fluorescence, showing hexagonal-close-packed order with spacing ~ 10 μm . **b**, Schematic block diagram of the microwave system used to drive qubit rotations. CPL, coupler; DRO, dielectric resonator oscillator;

IF, intermediate frequency; Mon, monitor; PLL, phase locked loop; Xtal osc., crystal oscillator. The 77 MHz reference is modulated for noise injection. **c**, Qubit transition driven via a square microwave π -pulse of $\tau_{\pi} \approx 185$ μs . **d**, Rabi oscillations driven on-resonance give a decay time of 30–40 ms. **e**, Ramsey fringes measured by detuning microwaves during free precession (filled blue symbols, 50 kHz, open red symbols, 100 kHz).

Doppler cooling of ion motion along the axis of the Penning trap²⁶, using ultraviolet laser light red-detuned from an atomic transition, yields ion temperatures of the order of 1 mK. State initialization occurs via optical pumping (Fig. 2a), and state readout is achieved by fluorescence detection on the same cycling transition used for cooling²⁷. We are able to initialize the system in a pure state with high fidelity, and perform a strong projective measurement, unlike some other ensemble techniques²⁸.

We employ pulse sequences consisting of a few to more than 1,000 π_X pulses. We have successfully extended our qubit coherence time (that is, $1/e$ decay time) from approximately 1 ms as measured via Ramsey free-induction decay, to over 200 ms using 500 π_X pulses in a CPMG sequence. In this study we focus primarily on sequences with $n \leq 10$, allowing us to compare pulse sequences in a regime where the minimum error rate is $\leq 1\%$.

We apply the CPMG and UDD sequences for various pulse numbers (Fig. 1a and d), and measure state decoherence due to ambient magnetic field fluctuations as a function of total free-precession time, as shown in Fig. 3a. The ambient magnetic field fluctuations in our high-field superconducting magnet are measured directly, giving an approximate $1/\omega^2$ spectrum ($S_\beta(\omega) \propto 1/\omega^4$) with additional sharp spurs of undetermined origin, including a prominent feature at ~ 153 Hz. The data in Fig. 3a demonstrate that it is possible to extend the qubit coherence time by adding π pulses, as expected. CPMG appears to perform similarly to UDD for all $n \leq 10$ in this noise environment, which has a soft high-frequency cut-off¹².

Fitting our experimental data requires that we account for finite π -pulse durations in expressions for the pulse sequence filter function, diverging from the zero-pulse-length assumptions made in most literature on dynamical decoupling^{13,29}. We assume that dephasing is negligible during the application of a π_X pulse, and build on the theoretical descriptions of refs 12 and 13. The above assumption leads to the insertion of a delay, length τ_π , between each free-precession time, during which the filter function in the time domain has value zero (rather than ± 1 ; refs 9, 13, 29). Moving to the frequency domain, we may write the filter function of an arbitrary n -pulse sequence as:

$$F(\omega\tau) = |\tilde{y}_n(\omega\tau)|^2 = \left| 1 + (-1)^{n+1} e^{i\omega\tau} + 2 \sum_{j=1}^n (-1)^j e^{i\delta_j\omega\tau} \cos(\omega\tau_\pi/2) \right|^2$$

where $\delta_j\tau$ is the time of the centre of the j th π_X pulse, and τ is the sum of the total free-precession time and π -pulse durations (Fig. 1b–d). To this order of approximation, all information pertaining to finite pulse lengths is accounted for by the simple addition of a cosine term in the equation.

Fits to experimental data show good agreement with theory. In Fig. 3a, the free fit parameters are the overall noise strength and the relative strength of the 153 Hz spur in our noise spectrum. This spur can be observed to slowly change amplitude in real time (on a time-scale of hours), and is entirely responsible for the plateau-like feature we see at intermediate times in our decoherence curves. Increasing the strength of this spectral feature changes the plateau-like feature to a rounded hill of increasing height. We believe that deviations between our experimental data and fitting functions are dominated by slow as well as discontinuous changes in the ambient noise environment.

Numerical simulations^{9,13} suggest that in the ‘high-fidelity regime’, UDD is capable of significantly outperforming CPMG in a variety of noise environments, suppressing errors by several orders of magnitude to yield ultimate fidelities in excess of 99.99%. In order to emphasize the performance differences between these sequences, we artificially inject noise to simulate systems where UDD outperforms CPMG in the lower-fidelity regime.

We inject noise with Ohmic and $1/\omega$ power spectra (see Supplementary Information) and test the relative performance of

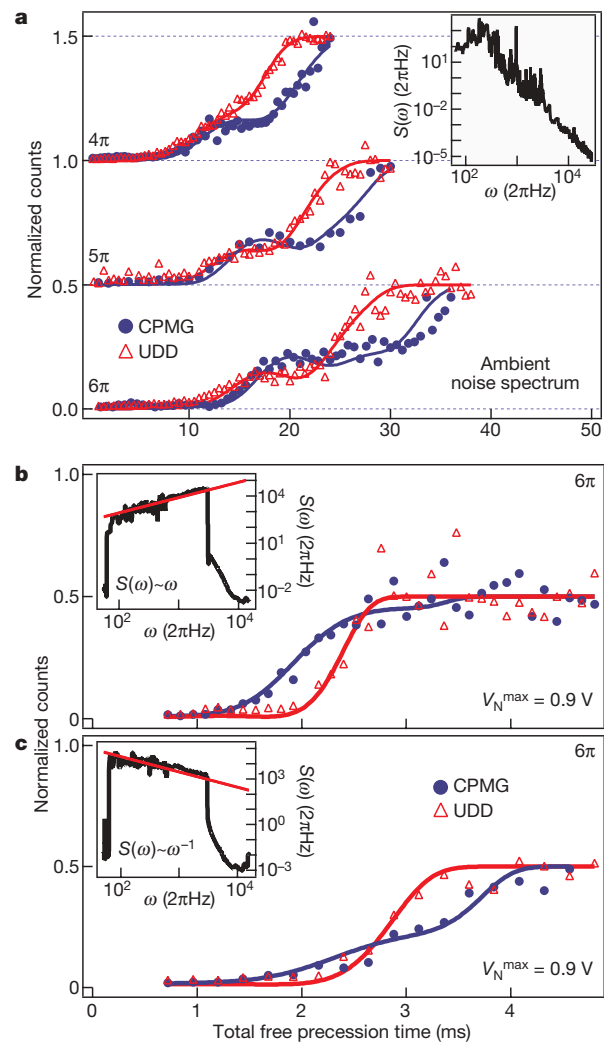


Figure 3 | Pulse sequence performance in the presence of various noise spectra. **a**, CPMG and UDD performance under ambient noise for various n . Phase errors manifested as non-zero fluorescence detection; traces saturate at 0.5 for total phase randomization. Traces for $n = 4, 5$ offset by 0.5 units for clarity. Each data point corresponds to 50 averages. Detailed fit parameters presented in Supplementary Information. Inset, ambient noise spectrum measured via a solenoid embedded in our NMR magnet. **b, c**, Performance of UDD and CPMG for noise spectrum displayed in respective inset with 500 Hz cut-off. UDD performance relative to CPMG improves with increasing noise intensity, as predicted by theory. Insets to **b** and **c** show smoothed noise on a log-log plot, measured using a phase-noise detection system with a noise modulation amplitude $V_N = 0.7$ V (Supplementary Information; red line represents intended noise envelope up to high-frequency cut-off).

UDD and CPMG (Fig. 3b and c). The peak injected noise power is approximately five orders of magnitude larger than the ambient spectrum; this extremely large noise power increases the overall error rates such that we may easily discern differences in sequence performance with limited measurement fidelity. Our data indicate that the UDD sequence dramatically outperforms CPMG in the presence of noise with an Ohmic spectrum and a sharp cut-off⁹—a significant departure from results under ambient noise. By contrast, using a $1/\omega$ power spectrum with a sharp cut-off, we find that over the entire range of accessible noise intensities, CPMG performs similarly to UDD. As expected, noise power at low frequencies is well-filtered by both sequences, yielding longer overall coherence times for the $1/\omega$ spectrum relative to the application of an Ohmic spectrum, and consistent with theoretical work¹². Theoretical fits using the appropriate noise spectrum and a single free parameter, α , a scaling factor for the overall noise level, again show good agreement with data.

A significant challenge for experimentalists employing dynamical decoupling techniques is derived from a general inability to precisely characterize $S_{\beta}(\omega)$. Realistic noise rarely resembles any simple idealized spectrum, as the specific measurement hardware and laboratory environment will add frequency components to $S_{\beta}(\omega)$ that are not easily measured or predicted by theory. Realizing optimal noise suppression therefore requires an ability to choose appropriate dynamical decoupling pulse sequences without precise knowledge of the noise environment.

We surpass previous efforts on dynamical decoupling sequence construction by developing novel locally optimized dynamical decoupling (LODD) pulse sequences that are tailored to a given experimental noise environment, and realized through real-time experimental feedback³⁰ without the need for any knowledge of the relevant noise spectrum. Our technique employs the Nelder-Mead simplex method for optimization in an n -dimensional space (n pulses), manipulating the relative pulse positions in a sequence for fixed sequence length (see Supplementary Information).

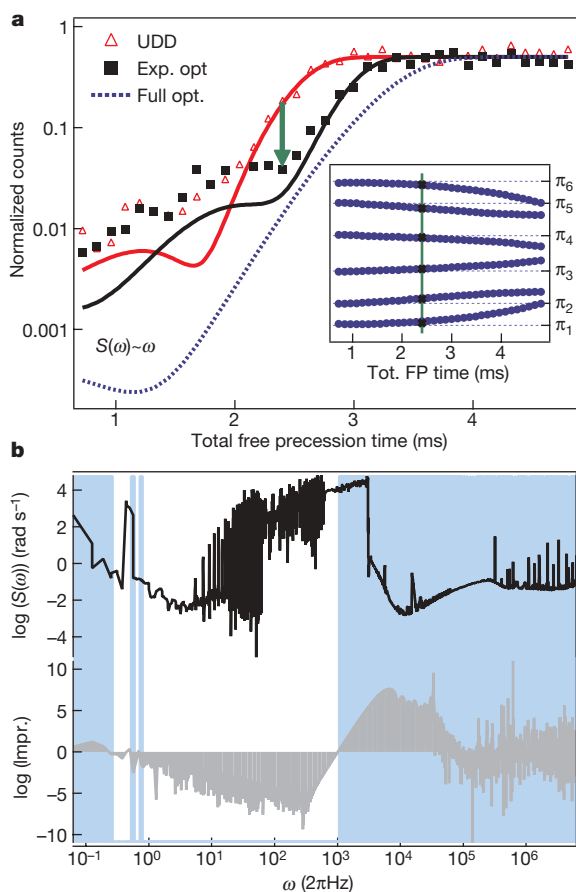


Figure 4 | Nelder-Mead pulse-sequence optimization using Ohmic spectrum and $n = 6$. **a**, UDD and experimentally optimized pulse sequence performance on a logarithmic scale. Green arrow indicates the sequence length for which experimental optimization was performed. Error suppressed $\sim 8\times$ relative to CPMG (not shown). Blue dotted line indicates simulated decoherence for sequences optimized at all τ and same noise strength as experimental optimization trace. Inset, optimized sequences for all values of total free-precession time (blue symbols). Black Xs indicate the π pulse positions of the single experimentally optimized sequence. Ticks and horizontal grids correspond to original UDD pulse positions. **b**, Filtration benefits of experimentally optimized pulse sequence tailored to injected noise environment. Noise power spectrum (upper trace) and logarithmic improvement of optimized filter function relative to UDD filter function (lower trace; grey shading highlights area). Positive numbers (also blue background shading) indicate regions of $S_{\beta}(\omega)$ where the optimized sequence provides noise suppression superior to UDD.

Experimental optimization results for an Ohmic spectrum are displayed in Fig. 4a, along with a schematic depiction of the resultant optimized pulse sequence as compared with UDD (Fig. 4a inset). Small modifications in the pulse positions (for both Ohmic and $1/\omega$ spectra) produce significant improvements for a given total free-precession time, and theoretical fits closely replicate experimental data. In the data presented, the LODD sequence suppresses the qubit error rate at the optimization point by a factor of five relative to UDD, and nearly an order of magnitude over CPMG. We believe that the divergence between data and theory below ~ 2 ms free-precession time is a consequence of the intrinsic noise floor in our measurement system, rather than a failure of the theory. The origin of the observed improvements is elucidated in Fig. 4b; the frequency range over which the LODD filter function is smaller than that for UDD overlaps with the spectral peak of the noise, thus reducing $\chi(\tau)$.

The experimental optimization shown in Fig. 4a is performed for only a single value of τ , suggesting that the limited range of τ over which the experimentally optimized sequence shows benefits is not fundamentally constrained. Indeed, numerical optimization for all values of τ yields a suite of LODD pulse sequences (Fig. 4a inset) that outperform CPMG and UDD in the high-fidelity regime by an order of magnitude (blue dashed line, Fig. 4a). Further, the experimentally optimized sequence is nearly identical to that derived numerically for the same value of the free precession time, validating the capabilities of our experimental optimization procedure.

In summary, we have demonstrated the efficacy of phase error suppression via optimized dynamical decoupling pulse sequences applied to a model quantum memory. This experimental system has been employed to test pulse sequences under a variety of experimentally realistic noise environments, yielding good agreement with theoretical predictions for qubit coherence. We have developed a real-time active feedback technique to experimentally produce locally optimized pulse sequences outperforming all others, without requiring any knowledge of the experimental noise environment. The strong agreement between data and theory under the application of extremely large noise power suggests that the use of dynamical decoupling pulse sequences should realistically be able to suppress qubit errors well below the fault-tolerance threshold under more commonly observed values of ambient noise power. Our results provide key ingredients of a quantum toolkit which will make the production of a functional and useful quantum computer more realistic, and apply broadly to all qubit technologies and unconstrained noise environments.

Received 18 December 2008; accepted 4 March 2009.

- Nielsen, M. A. & Chuang, I. L. *Quantum Computation and Quantum Information* (Cambridge Univ. Press, 2000).
- Zoller, P. *et al.* Quantum information processing and communication — strategic report on current status, visions and goals for research in Europe. *Eur. Phys. J. D* **36**, 203–228 (2005).
- Haeberlen, U. *High Resolution NMR in Solids* (Advances in Magnetic Resonance Series, Academic, 1976).
- Viola, L. & Lloyd, S. Dynamical suppression of decoherence in two-state quantum systems. *Phys. Rev. A* **58**, 2733–2744 (1998).
- Zanardi, P. Symmetrizing evolutions. *Phys. Lett. A* **258**, 77–82 (1999).
- Vitali, D. & Tombesi, P. Using parity kicks for decoherence control. *Phys. Rev. A* **59**, 4178–4186 (1999).
- Byrd, M. S. & Lidar, D. A. Empirical determination of dynamical decoupling operations. *Phys. Rev. A* **67**, 012324 (2003).
- Khodjasteh, K. & Lidar, D. A. Fault-tolerant quantum dynamical decoupling. *Phys. Rev. Lett.* **95**, 180501 (2005).
- Uhrig, G. Keeping a quantum bit alive by optimized π -pulse sequences. *Phys. Rev. Lett.* **98**, 100504 (2007).
- Vandersypen, L. M. K. & Chuang, I. NMR techniques for quantum control and computation. *Rev. Mod. Phys.* **76**, 1037–1069 (2004).
- Witzel, W. & Das Sarma, S. Multiple-pulse coherence enhancement of solid state spin qubits. *Phys. Rev. Lett.* **98**, 077601 (2007).
- Uhrig, G. Exact results on dynamical decoupling by π pulses in quantum information processes. *N. J. Phys.* **10**, 083024 (2008).
- Cywinski, L., Lutchny, R., Nave, C. & Das Sarma, S. How to enhance dephasing time in superconducting qubits. *Phys. Rev. B* **77**, 174509 (2008).
- Yao, W., Liu, R. B. & Sham, L. J. Restoring coherence lost to a slow interacting mesoscopic spin bath. *Phys. Rev. Lett.* **98**, 077602 (2007).

15. Zhang, W. *et al.* Long-time electron spin storage via dynamical suppression of hyperfine-induced decoherence in a quantum dot. *Phys. Rev. B* **77**, 125336 (2008).
16. Yang, W. & Liu, R. B. Universality of Uhrig dynamical decoupling for suppressing qubit pure dephasing and relaxation. *Phys. Rev. Lett.* **101**, 180403 (2008).
17. Kuopanportti, P. *et al.* Suppression of $1/f^2$ noise in one-qubit systems. *Phys. Rev. A* **77**, 032334 (2008).
18. Lee, B., Witzel, W. & Das Sarma, S. Universal pulse sequence to minimize spin dephasing in the central spin decoherence problem. *Phys. Rev. Lett.* **100**, 160505 (2008).
19. Faoro, L. & Ioffe, L. B. Quantum two level systems and Kondo-like traps as possible sources of decoherence in superconducting qubits. *Phys. Rev. Lett.* **96**, 047001 (2006).
20. Koch, R. H., DiVincenzo, D. P. & Clarke, J. Model for $1/f$ flux noise in SQUIDs and qubits. *Phys. Rev. Lett.* **98**, 267003 (2007).
21. Leggett, A. J. *et al.* Dynamics of the dissipative two-state system. *Rev. Mod. Phys.* **59**, 1–85 (1987).
22. Taylor, J. M. & Calarco, T. Wigner crystals of ions as quantum hard drives. *Phys. Rev. A* **78**, 062331 (2008).
23. Itano, W. M. *et al.* Bragg diffraction from crystallized ion plasmas. *Science* **279**, 686–689 (1998).
24. Mitchell, T. B. *et al.* Direct observations of structural phase transitions in planar crystallized ion plasmas. *Science* **282**, 1290–1293 (1998).
25. Huang, X.-P., Bollinger, J. J., Mitchell, T. B. & Itano, W. M. Phase-locked rotation of crystallized non-neutral plasmas by rotating electric fields. *Phys. Rev. Lett.* **80**, 73–76 (1998).
26. Jensen, M. J., Hasegawa, T., Bollinger, J. J. & Dubin, D. H. E. Rapid heating of a strongly coupled plasma near the solid-liquid phase transition. *Phys. Rev. Lett.* **94**, 025001 (2005).
27. Brewer, L. R. *et al.* Static properties of a non-neutral ${}^9\text{Be}^+$ ion plasma. *Phys. Rev. A* **38**, 859–873 (1988).
28. Itano, W. M. *et al.* Quantum projection noise: Population fluctuations in two-level systems. *Phys. Rev. A* **47**, 3554–3570 (1993).
29. Pasini, S., Fischer, T., Karbach, P. & Uhrig, G. Optimization of short coherent control pulses. *Phys. Rev. A* **77**, 032315 (2008).
30. Weinacht, T. C. & Bucksbaum, P. H. Controlling the shape of a quantum wavefunction. *Nature* **397**, 233–235 (1999).

Supplementary Information is linked to the online version of the paper at www.nature.com/nature.

Acknowledgements We thank L. Cywinski, S. Das Sarma, V. V. Dobrovitski, X. Hu, E. Knill, S. Lyon, G. Uhrig, and W. Witzel for discussions. We also thank D. Hanneke, C. Ospelkaus and D. J. Wineland for comments on the manuscript, and C. Nelson for technical assistance. We acknowledge research funding from IARPA and the NIST Quantum Information Program. M.J.B. acknowledges fellowship support from IARPA and Georgia Tech., and H.U. acknowledges support from CSIR. This manuscript is a contribution of the US NIST and is not subject to US copyright.

Author Information Reprints and permissions information is available at www.nature.com/reprints. Correspondence and requests for materials should be addressed to M.J.B. (biercuk@boulder.nist.gov).